
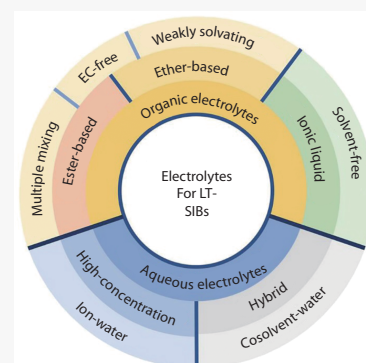


A perspective on low-temperature electrolytes for sodium-ion batteries

Tianze Shi^{1,2,§}, Ruilin Hou^{1,2,§} and Shaohua Guo^{1,2*} 

As an ideal candidate for the next generation of energy storage devices, sodium-ion batteries (SIBs) have received tremendous attention in recent years. However, the more extensive and harsh application environment puts forward higher requirements for the low-temperature SIBs, which is mainly limited by electrolyte-related sluggish ion transport at low temperature. This perspective focuses on the low-temperature electrolytes of SIBs, and provides the in-depth understanding of the failure reasons of organic and aqueous electrolytes in SIBs at low temperature. Then, the research progress in the low-temperature organic/aqueous electrolytes are comprehensively summarized and systematically analyzed. This review is conducted to enable the rational design of low-temperature electrolytes and further promote the development of all-climate SIB technology.



As a potential alternative for lithium-ion batteries (LIBs), sodium-ion batteries (SIBs) have broad application prospects in large-scale power grid energy storage, mopeds, and other fields due to their similar electrochemical properties to LIBs as well as abundant sodium metal resources and low cost.^[1–5] Predictably, the increasingly mature SIB technology is bound to face a broader application field and a worse working environment, especially extreme low temperature conditions, such as high latitude/altitude area, outer space exploration and underwater operation.^[6–12] However, the research of low-temperature (LT) SIB technology is still in infancy. It is necessary and urgent to have an in-depth understanding and comprehensive review of LT-SIBs technology.

There are several key factors that limit the development of LT-SIBs, such as the decrease in electrode reaction rate, changes in electrode material properties, high freezing point of electrolytes, reduced electrolyte ionic conductivity, and decreased migration ability of Na⁺. Currently, most of the research on LT-SIBs focused on the electrode materials design, including the construction of three-dimensional ionic chan-

nels^[13–19], optimization of electronic conductivity^[20–24] and electrode kinetics enhancement^[25–29], as shown in Table 1. The purpose of all above strategies is facilitating the sluggish solid-diffusion process of Na⁺ and improving the contact between electrode materials and electrolyte at LT. However, the optimization of LT performance of SIBs by modifying electrode materials is very limited. In addition, the LT performance of SIBs can also be improved to some extent by artificially designing the electrode/electrolyte interface.^[30–33] Obviously, both electrode optimization and artificial interface are not only difficult to operate, but also will greatly increase the production cost of SIB, which is not friendly to industrial production. Inspired by LT-LIBs technology, we can know that the slow ion transport associated with the electrolyte at LT is the main reason for limiting the LT performance of the battery.^[34–36] In addition, the design of LT electrolyte is more suitable for industrial production of SIB and the cost is controllable.

In terms of the LT-SIBs, the main problems they faced at LT are the low ionic conductivity of bulk electrolyte, high desolvation energy and sluggish Na⁺ diffusion kinetics in the electrode/electrolyte interface.^[37,38] Specifically, the viscosity of the electrolyte inevitably increases and the ionic conductivity decreases accordingly at LT, resulting in the slow transport of Na⁺ in the bulk electrolyte.^[39,40] Then, the solvated Na⁺ will undergo desolvation before entering the electrode material.^[41] The high desolvation energy at LT greatly limits the ion transport rate, which is proved to be the rate-controlling step of ion transport at LT.^[42,43] Although some studies attempted to circumvent this problem, they faced to the severe volume change of the electrode materials caused by the co-

¹ Shenzhen Research Institute of Nanjing University, Shenzhen 518000, China

² College of Engineering and Applied Sciences, Jiangsu Key Laboratory of Artificial Functional Materials, National Laboratory of Solid State Microstructures, Collaborative Innovation Centre of Advanced Microstructures, Frontiers Science Center for Critical Earth Material Cycling, Nanjing University, Nanjing 210093, China

* Corresponding author, E-mail: shguo@nju.edu.cn

Received 31 January 2023; Accepted 10 May 2023; Published online

§These authors contributed equally to this work.

Table 1. The comparison of LT performance of various electrode materials for SIBs.

Electrode Design Strategies	Electrolytes	Cathode Anode	Lowest Operation Temperature (°C)	Specific Capacity (mAh g ⁻¹)	Capacity Retention/Number of Cycles	Ref.
The Construction of Three-dimensional Ionic Channels	1 M NaClO ₄ in PC 5vol%FEC	Ca-doped Na ₃ V ₂ (PO ₄) ₃ (CNVP@C/3DNC-0.1) Na	0	112.3	96.3%/500 1 C	[13]
	1 M NaClO ₄ in EC/DEC (1:1 vol)	MoS ₂ @MXene@D-TiO ₂ Na	-30	253 50 mA g ⁻¹	-/100 50 mA g ⁻¹	[14]
	1 M NaClO ₄ in PC/EC (1:1 vol) 5vol%FEC	Na ₃ V ₂ (PO ₄) ₃ /C NaTi ₂ (PO ₄) ₃ /C	-20	60 1 C	-/1000 10C/20 C	[14]
	1 M NaClO ₄ in PC/EC 5wt%FEC	3D Se/graphene composite Na	-25	259 0.05 A g ⁻¹	1000 2 A g ⁻¹	[18]
	1 M NaPF ₆ in PC/EMC 5vol%FEC	carbon-coated Fe ₃ BO ₅ Na	-40	292 50 mA g ⁻¹	—	[21]
Optimization of Electronic Conductivity	1 M NaPF ₆ in PC/EMC 5vol%FEC	Na ₃ Fe ₂ (PO ₄) ₂ (P ₂ O ₇)@rGO carb on-coated Fe ₃ BO ₅	-40	45.1 0.5 C	-/20 0.1 C	[21]
	1 M NaCF ₃ SO ₃ in DEGDME	FePSe ₃ Na	-30	230 5 A g ⁻¹	-/3000 5 A g ⁻¹	[20]
	1 M NaClO ₄ in PC 5vol%FEC	NaFePO ₄ @C Na	-10	114.1 0.1 C	-/1000 2 C	[22]
	1 M NaClO ₄ in PC 5vol%FEC	NaFePO ₄ @C Na	-20	103.8 0.1 C	-/1000 2 C	[22]
	1 M NaPF ₆ in diglyme	Na _{0.8} Fe _{0.8} Ti _{1.2} O ₄ Na	-20	70 0.2 C	—	[23]
Electrode Kinetics Enhancement	1 M NaCF ₃ SO ₃ in diglyme	Ti ₃ C ₂ -N _{funct} Na	-25	201 0.05 A g ⁻¹	80.9%/5000 1 A g ⁻¹	[25]
	0.5 M NaCF ₃ SO ₃ in DME	CoGa ₂ S ₄ @G Na	-60	2 nd 361.2 0.2 A g ⁻¹	-/1000 1 A g ⁻¹	[28]
	1 M NaCF ₃ SO ₃ in diglyme	TiO ₂ -B/anatase Na	-25	122 10 C	-/1000 10 C	[47]

intercalation/extraction behavior during the charging-discharging process and the limitation of material selection.^[26,27,44] In addition, the LT performance of SIBs will also be affected by the slow ion diffusion in solid electrolyte interphase (SEI), whose component and structure depend on the electrolyte formula.^[45,46] Obviously, the design of LT electrolyte plays a key role in improving the LT performance of SIBs.

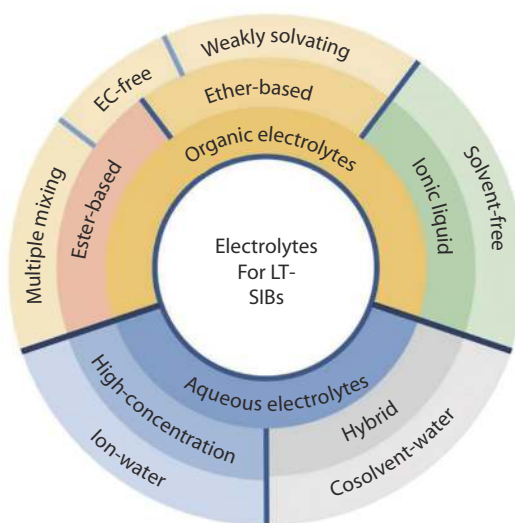
Here, we attempt to break through the bottleneck of LT performance of SIBs from the aspect of electrolyte optimization (Figure 1). Firstly, the reasons that limit the LT performance of organic electrolyte are analyzed, and the property requirements and design criteria of LT organic electrolyte for SIBs are proposed. And the research progress of ester-based, ether-based and ionic liquid LT electrolytes are summarized, comprehensively. Then, the LT failure mechanism of aqueous electrolyte is analyzed, and its application potential in LT-SIBs is pointed out. The design strategies of LT aqueous electrolyte are summarized from two aspects of high-concentration and hybrid electrolytes. Finally, we provide promising re-

search strategies and pathways towards improving the LT performance of SIBs from the perspective of electrolyte design in the future.

Organic Electrolytes

Fundamental of LT Organic Electrolyte

Research on LT electrolytes for SIBs has been gaining momentum over the past decade. Initially, from 2018 to 2020, the main strategies employed to reduce the freezing point of organic electrolytes were to add functional additives or use EC-free solvents. Recently, some new strategies have been proposed to further lower the freezing point of the electrolyte and enhance its ion conductivity at LT. For instance, a method combining multiple solvents was proposed in 2020 by Liu et al.^[48], and the weak solvation strategies emerged in 2022, which further accelerated the interfacial ion kinetics at LT. Through above strategies, the sodium-ion electrolytes have achieved lower freezing point, resulting to improved LT

**Fig. 1** Electrolyte design strategies for LT-SIBs.

performance in SIBs. In the initial stages, in order to meet the needs of anode for the reduction stability of electrolyte, organic electrolyte is the preferred electrolyte for SIBs. To obtain high ionic conductivity of organic electrolyte, high polar organic solvent is usually selected, which can effectively dissociate sodium salt through strong ion-solvent interactions. For example, inspired by the commercial electrolyte of LIBs, cyclic ethylene carbonate (EC) is selected to dissolve NaPF_6 , resulting to the electrolyte of SIBs.^[49] However, due to the high viscosity of EC, the conductivity of single EC electrolyte cannot meet the requirements of SIBs at room temperature, let alone the harsh LT environment.^[50] Even if diluted by conventional low polarity solvent, the ionic conductivity of EC-based organic electrolyte will rapidly decrease with the temperature, which undoubtedly seriously affects the LT performance of sodium-ion electrolyte.^[51,52] In addition, in Na^+ organic electrolyte, Na^+ usually exists in bulk electrolyte in the form of solvated ion, while its storage in electrode material is mainly in the form of bare ion. Therefore, solvated ions usually need to be desolvated at the electrode-electrolyte interface, which has been proved to be the rate-limiting step of ion transport at LT.^[53–55] If there is SEI/CEI film at the interface, the bare ion diffusion rate across SEI/CEI film will also affect the ion transport kinetics.^[56–59] Generally, the diffusion rate of cations in SEI/CEI films is typically determined by their composition and structure. The inorganic-rich SEI/CEI films tend to exhibit higher ionic conductivity compared with organic-rich SEI/CEI, with the conductivity generally following the trend of nitrides > fluorides > oxides. In addition, the thinner SEI/CEI films have shorter ion diffusion distances, which are conducive to achieving faster ion transport. It is well-known that SEI/CEI is derived from the decomposition of the electrolyte at the interface. Therefore, the composition and structure of SEI/CEI films can be regulated by adjusting the component and solvation structure of the electrolyte. In summary, whether the objective is to reduce the freezing point of the electrolyte or optimize the ion diffusion rate at the interface, both of them can be optimized by electrolyte designing.

To this end, the ideal LT organic electrolyte should have high LT ionic conductivity, low LT desolvation energy and fast LT ionic diffusion rate in SEI/CEI film. The design of LT organic electrolyte should follow the following requirements, theoretically. First, the organic electrolytes should have the lowest possible freezing point, which can ensure that they have sufficient charge-carrier ions concentration at LT. Second, the solvation structure of the electrolyte should have a weak solvation energy, which can accelerate the ion desolvation process at LT.^[60] Finally, the LT organic electrolyte should be able to derive a thin and inorganic-rich SEI/CEI film, which can ensure the basic role of the film while shortening the ion diffusion distance and accelerating the ion diffusion rate. In fact, the research of LT Na^+ organic electrolyte has always followed the above principles, which will be reviewed in detail in the following section.

Advances in developing in LT Organic Electrolyte

Ester-based Electrolytes

Carbonate based solvents, especially EC, are the most widely used organic solvents in commercial SIB, due to their high solubility, excellent high-voltage oxidation stability and

low-voltage SEI film forming ability. However, their high viscosity at LT has greatly damaged the LT performance of SIBs. Generally, the ionic conductivity and viscosity of EC-based electrolyte at LT can be effectively improved by mixing with low-freezing point solvent, such as propylene carbonate (PC)^[63], diethyl carbonate (DEC)^[64,65] and ethyl methyl carbonate (EMC)^[66]. For example, when the temperature lower than $-10\text{ }^\circ\text{C}$, the conductivity of EC-based electrolyte (1.0-EP:1.0 M NaPF_6 in EC/PC, 1:1 by vol) decrease and its viscosity increase, evidently (Figure 2a and 2b). With the increase of dilution degree (0.8 M NaPF_6 in FEC/EMC/HFE, 3:3:4 by vol), its LT conductivity and viscosity have been effectively improved. It is noteworthy that it is feasible to classify this electrolyte as either a weakly solvating electrolyte or a localized high-concentration electrolyte. On the one hand, the HFE solvent is indeed a commonly used diluent that does not directly interact with cations/anions in the electrolyte. Therefore, the above electrolyte can be classified as a localized high-concentration electrolyte.^[67] On the other hand, as the main solvent, FEC also serves as the primary solvent for dissolving sodium salts and forms weak solvating structures with Na^+ . Therefore, the above electrolyte could also belong to weakly solvating electrolyte. Subsequently, various binary or ternary-solvent electrolytes are broadly used in the SIBs. Except to improving the ionic conductivity of the LT electrolyte, some functional additives can be used to optimize the ion transport rate at interface. For instance, Song et al.^[64] developed a kind of electrolyte of 1.0 M NaPF_6 in EC/DEC/PC (1:2:1 by vol) with 5 vol% fluoroethylene carbonate (FEC) and 3 vol% adiponitrile (ADN) as additives. The $\text{Na}_{0.76}\text{Ni}_{0.3}\text{Fe}_{0.4}\text{Mn}_{0.3}\text{O}_2 \parallel \text{hard carbon (HC)}$ pouch cell using this kind electrolyte achieved 76.45% room-temperature (RT) discharge capacity retention at $-20\text{ }^\circ\text{C}$ in 0.2 C.

According to the previous analysis, EC is the main component that causes the poor LT performance of the EC-electrolyte. Therefore, the development of other main-solvents to replace EC is expected to further reduce the freezing point of the electrolyte and the operating temperature of SIBs. Among various commonly used ester-based solvents, PC can replace EC as the main-solvent of SIB because of its good compatibility with HC anode. Thanks of its low freezing point of $-49\text{ }^\circ\text{C}$, PC-based electrolyte can obtain excellent LT performance. For instance, Che et al.^[48] tested pouch cells ($\text{NaNi}_{1/3}\text{Fe}_{1/3}\text{Mn}_{1/3}\text{O}_2 \parallel \text{HC}$) with 1.0 M NaPF_6 in PC/EMC (1:1 by vol) as electrolyte and discovered that the RT capacity retentions of these cells reached 52.16% at $-40\text{ }^\circ\text{C}$ (Figure 2c). In addition, fluorinated solvent is another excellent alternative to EC for the design of LT electrolyte (Figure 2d). Compared to non-fluorinated solvents, fluorinated solvents have many advantages in LT electrolytes.^[68] On the one side, due to the strong electronegativity of the fluorine atom, fluorinated solvents have weaker solvation ability, leading to weaker intermolecular forces and potentially lower freezing points. On the other side, the C-F bond has a lower LUMO energy level, making fluorinated solvents more likely to form a SEI containing fluorinated inorganic compounds by reduction on the electrode surface, which has a higher ionic conductivity than the EC-derived carbonate SEI. For example, Liu et al.^[62] designed an EC-free electrolyte with a formula of 1.0 M NaTFSI -FEC/FEMC/fluorobenzene (FB) (3:3:4 by vol), which exhibited the lower freezing point of $-50.5\text{ }^\circ\text{C}$. First of all, compared with EC, the fluorin-

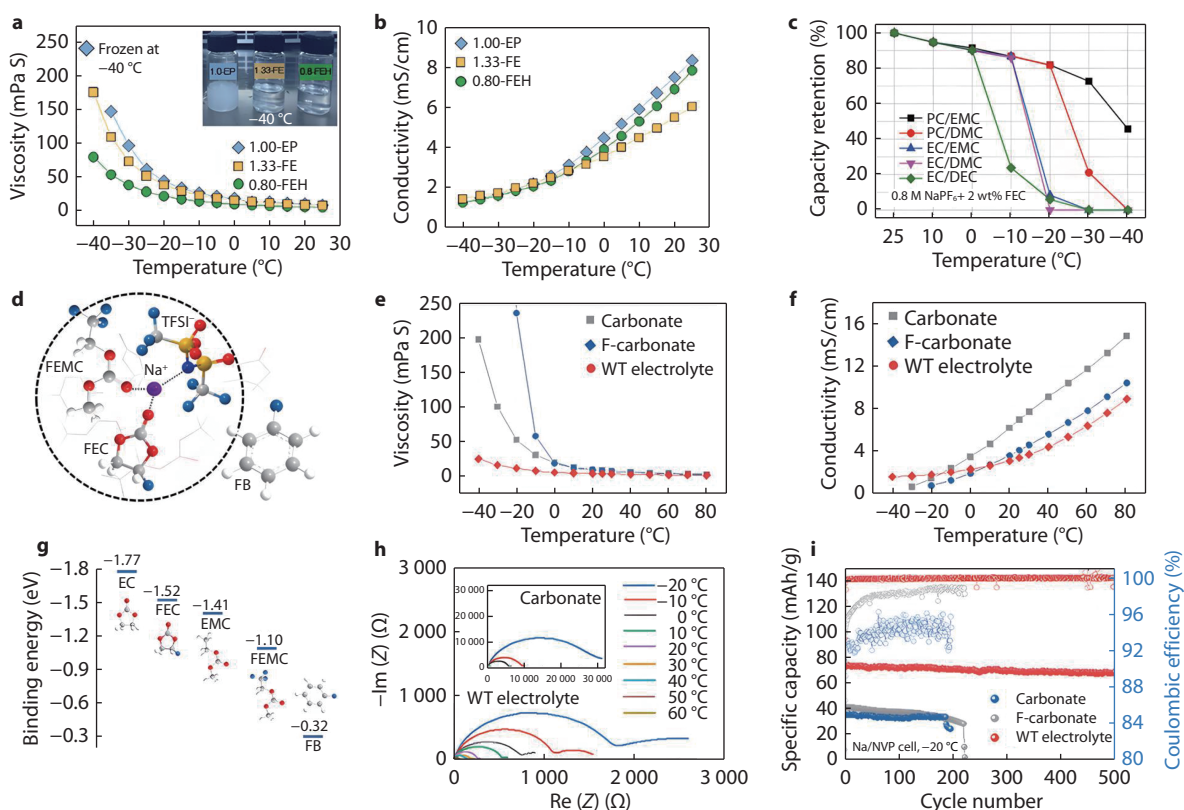


Fig. 2 **a** Ionic conductivity and **b** viscosity of EC-based electrolytes changes from $-40\text{ }^{\circ}\text{C}$ to $30\text{ }^{\circ}\text{C}$.^[61] Copyright 2021, Elsevier. **c** Capacity retention of pouch cells with EC-based and EC-free electrolytes at various temperatures.^[48] Copyright 2021, Elsevier. **d** Representative solvation structure conducted by MD simulations. **e** Viscosity and **f** ionic conductivity of different electrolytes changes from $-40\text{ }^{\circ}\text{C}$ to $80\text{ }^{\circ}\text{C}$. **g** The binding energy between Na^+ and corresponding solvents. **h** Nyquist plots and EIS fitting for the $\text{Na} \parallel \text{Na}$ symmetric cells of EC-based electrolyte and WT electrolyte from $-20\text{ }^{\circ}\text{C}$ to $60\text{ }^{\circ}\text{C}$ after 3 formation cycles. **i** Cycling performance of $\text{Na}_3\text{V}_2(\text{PO}_4)_3 \parallel \text{Na}$ cells with different electrolytes at 0.5 C , $-20\text{ }^{\circ}\text{C}$.^[62] Copyright 2022, Elsevier. (1.0-EP: 1.0 M NaPF_6 in EC/PC, 1:1 by vol; 1.33-FE: 1.33 M NaPF_6 in FEC/EMC, 1:1 by vol; 0.8-FEH: 0.8 M NaPF_6 in FEC/EMC/HFE, 3:3:4 by vol).

ated carbonate main-solvents have low freezing points (FEC, $20\text{ }^{\circ}\text{C}$). Moreover, co-solvent FB had low freezing point of $-42\text{ }^{\circ}\text{C}$, which was beneficial to maintain low viscosity (Figure 2e) and high ionic conductivity (Figure 2f) of the electrolyte at subzero temperature. Meanwhile, as an inert diluent, FB could weaken the coordination of Na^+ -solvent (Figure 2d and 2g), resulting in alleviating the decomposition of solvent molecules on the sodium metal anode (SMA) surface. As a result, an organic-inorganic adaptive thin SEI formed on the SMA surface at $-20\text{ }^{\circ}\text{C}$, which renders a 16-fold decrease of cell impedance and induced the dense Na deposition in comparison with the conventional EC-based electrolyte (Figure 2h). In addition, as shown in Figure 2i, the $\text{Na}_3\text{V}_2(\text{PO}_4)_3 \parallel \text{Na}$ half-cell with this EC-free electrolyte exhibited a discharge capacity of 73.9 mAh g^{-1} , 72.8% of the RT capacity, which is much higher than that of the EC-based (35.5 mAh g^{-1}) and F-carbonate (39.9 mAh g^{-1}) electrolytes. In addition, the longer lifespan (500 cycles) and high CE (99.6%) at $-20\text{ }^{\circ}\text{C}$ also proved that the EC-free electrolyte design strategy is effective. Similar electrolyte design strategy was also applied to other LT electrolytes, such as 0.8 M NaPF_6 in FEC/EMC/HFE (3:3:4 by vol)^[66] and 0.58 M NaBOB-NMP/TMP (1:1 by vol)^[69] as shown in Table 2.

Generally, commonly used ester-based solvents have high polarity and poor LT performance. In addition, they are prone

to form SEI primarily composed of carbonates, which has poor conductivity. Furthermore, ester-based solvents have poor compatibility with high-capacity SMAs, which limits their potential use in LT sodium metal batteries. However, they usually exhibit excellent high-voltage stability.

Ether-based Electrolytes

As analyzed in section 2.1, the ideal LT electrolyte should have high ionic conductivity, low solvation energy and fast ion diffusion rate within SEI film. All of them point to weak solvation in theory. For the electrolyte of SIB with fixed charge-carrier ion type, the strength of solvation energy depends on the selected organic solvent. Compared to ester-based solvents, ether-based solvents have lower polarity, generally, which implies the lower freezing points.^[73] Therefore, the ether-based solvents are preferentially chosen to reduce the solvation/desolvation energy.^[58,74,75] The relevant mechanism has been fully demonstrated in the development of LT electrolytes for LIBs.^[76] Thus, ether-based electrolytes have advantages at LT in theory. For example, Wang et al.^[71] formulated a weakly solvating electrolyte comprising linear/cyclic ethers (diethylene glycol dimethyl ether (DEGDME)/1,3-dioxolane (DOL)) with the freezing point below $-150\text{ }^{\circ}\text{C}$ (Figure 3a and 3b). Meanwhile, Figure 3c showed that 0.5 M NaOTf-DEGDME/DOL (2:8) presented the slowest de-

Table 2. The comparison of LT performance of ester-based electrolytes for SIBs.

Electrolytes	Freezing Point (°C)	Cathode Anode	Lowest Operation Temperature (°C)	Specific Capacity (mAh g ⁻¹)	Capacity Retention/ Number of Cycles	Ref.
0.3 M NaClO ₄ -EC/PC (1:1 vol) 5%FEC	–	Na ₃ V ₂ (PO ₄) ₂ F ₃ Na	–25	109.7 0.2 C	94.1%/500 1 C	[63]
0.3 M NaClO ₄ -EC/PC (1:1 vol) 5%FEC	–	Na ₃ V ₂ (PO ₄) ₂ F ₃ HC	–25	–	91%/50 0.2 C	[63]
1 M NaPF ₆ -EC/DEC/PC (1:2:1 vol) with 5 vol% FEC and 3 vol% adiponitrile (ADN)	<–40	Na _{0.76} Ni _{0.3} Fe _{0.4} Mn _{0.3} O ₂ HC	–20	76.45% of RT 0.2 C	–	[64]
0.8 M NaPF ₆ in FEC/EMC/HFE(TTE) (3:3:4 vol)	–	Na ₃ V ₂ (PO ₄) ₂ F ₃ Na-SF	–20/–30	–30 °C 92.1 0.2 C	–20 °C 88.7%/600 0.5 C	[66]
1 M NaPF ₆ -PC/EMC (1:1 vol) with 2 wt% FEC	<–40	NaNi _{1/3} Fe _{1/3} Mn _{1/3} O ₂ HC	–40	52.16% of RT	–	[48]
1 M NaTFSI/FEC-FEMC-FB (3:3:4 vol)	–50.5	Na ₃ V ₂ (PO ₄) ₃ Na	–20	73.5 0.5 C	–/500 0.5 C	[62]
0.58 M NaBOB-NMP/TMP (1:1 vol)	<–90	–	–	–	–	[69]
1 M NaPF ₆ -PC/EA (1:1 vol) with 0.5 vol% VC	<–40	C(Mo ₂ C) C(Mo ₂ C)	–40	–	–	[70]

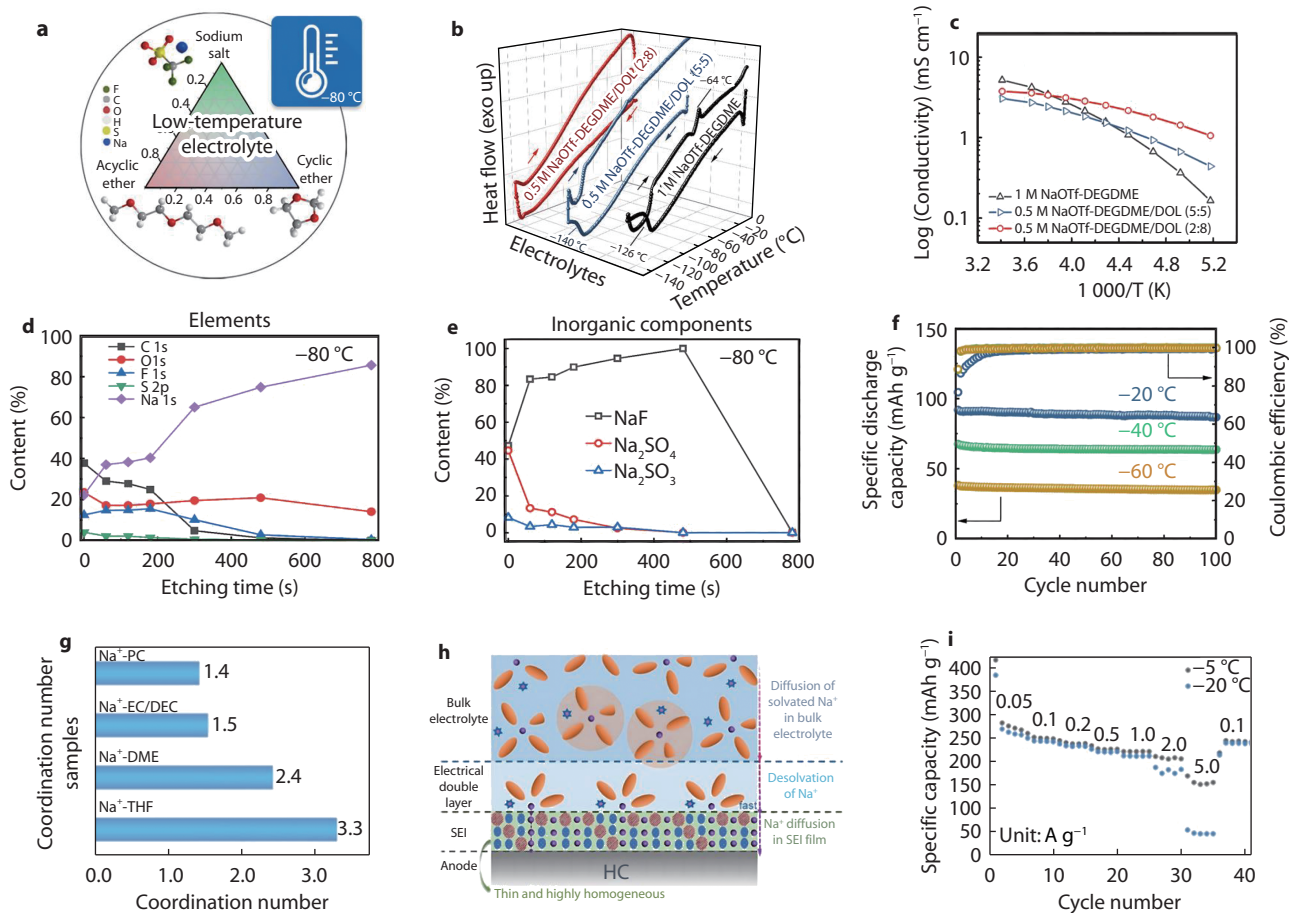


Fig. 3 **a** Schematic diagram of LT weakly solvating electrolyte comprising NaOTf and DEGDME/DOL mixed solvent. **b** Heat flow of different electrolytes from 0°C to -150°C . **c** Temperature-dependent ionic conductivity of different electrolytes. Contents of **d** elements and **e** inorganic components in the SEI at -80°C . **f** Cycling performance of $\text{Na}_3\text{V}_2(\text{PO}_4)_3 || \text{Na}$ cells at 22 mA g^{-1} at various temperatures. [71] Copyright 2022, Springer Nature. **g** Coordination numbers of 1 M NaPF_6 in THF, DME, EC/DEC and PC. **h** Schematic diagram of ion transport in THF electrolyte and SEI. **i** Rate performance of HC || Na cells at -5°C and -20°C . [72] Copyright 2022, Wiley-VCH.

crease in the ionic conductivity with temperature. It is worth knowing that the above electrolyte exhibited a unique weakly solvation structure. On the one side, the Na^+ solvation ability of DOL is lower than that of DEGDME. Thus, the electrolyte with high DOL proportion must exhibit a weak solvating structure in the form of weak Na^+ -DOL coordination [77], which is beneficial to reduce the desolvation energy at LT, effectively. On the other side, weak solvation enhances the cation-

anion interaction in the Na^+ solvation structure, which promotes the OTf⁻ reduction on the SMA surface, leading to the formation of a robust NaF-rich SEI with strong mechanical strength and high ion diffusion rate (Figure 3d and 3e). Therefore, the $\text{Na}_3\text{V}_2(\text{PO}_4)_3 || \text{Na}$ half-cell using the above electrolyte exhibited a specific capacity of about 40 mAh g^{-1} at 0.2 C at -60°C , and achieved a high CE (99.5%) and capacity retention (91%) after 100 cycles (Figure 3f). In addition, other ether-

based solvents were also used to design weakly solvating electrolytes to achieve excellent LT performance. Mixed solvents containing tetrahydrofuran (THF) have also been proved to have significant gains for the construction of weakly-solvated structures. For instance, Zhou et al.^[78] designed the Na⁺-based weakly solvating electrolyte using THF, THF/1,2-dimethoxyethane (DME) (3:1 by vol), which significantly mitigates the kinetic barrier for Na⁺ desolvation at LT. Furthermore, an anion-derived NaF-rich SEI film generated on the SMA suppresses the dendrite growth and guarantees stable cycling of SMBs down to −60 °C. The NaTi₂(PO₄)₃ || Na half-cell with 0.8 M NaOTf in the THF₃/DME₁ (3:1 by vol) as electrolyte delivered an initial capacity of 88.8 mAh g^{−1} at 1C at −20 °C (93.57% RT capacity retention). In addition, Tang et al.^[72] had proved that ether-based weakly solvating electrolyte could also hugely improve the LT performance of HC anode for SIBs. As shown in Figure 3g, compared with the common ester-based solvents (PC, EC/DEC) or liner ether-based solvents (DME), the Na⁺ had higher coordination number for THF solvent, which implied lower solvation energy. Thus, the coordinated Na⁺ could desolvated on the electrode surface rapidly. At −20 °C, the HC || Na half-cell with 1.0 M NaPF₆ in THF as electrolyte exhibited a high capacity of 269 mAh g^{−1} at 20 mA g^{−1} (Figure 3i) and a capacity retention of up to 95% with a specific capacity of 181 mAh g^{−1} over 1000 cycles at 2A g^{−1}. At present, a series of ether-based weakly solvating elec-

trolites for SIBs have been developed and exhibit excellent LT performance, including 0.5 M NaPF₆ in DEGDME^[79] and 0.3 M NaPF₆ in DEGDME/THF^[80] as shown in Table 3. The key to designing weakly solvating electrolytes lies in constructing weakly solvating structures that reduce the interaction between cations and solvents. Thus, the cationic desolvation energy at the interface is lowered, leading to accelerated interfacial dynamics. Additionally, by allowing more anions to coordinate with the cations, anions can preferentially undergo reduction at the interface, generating an inorganic-rich SEI and speeding up the diffusion of cations at the interphase. When selecting solvents for weakly solvating electrolytes, it is crucial to find a balance between "solvation energy" and "solubility". In other words, it requires reducing the interaction between the solvent and charge carriers while ensuring decent carrier concentration. The selection of solvents can be based on reference values of the donor number and dielectric constant. According to the latest research from Wang et al.^[60], solvents with a relatively low donor number (less than 10) and high dielectric constant (greater than 5) can be used for weakly solvating electrolytes. In addition, the type of functional groups in the solvent should also be taken into consideration. For instance, fluorinated solvent can facilitate the formation of inorganic-rich SEI, which can enhance the LT performance of batteries.

Table 3. The comparison of LT performance of ether-based electrolytes for SIBs.

Electrolytes	Freezing Point (°C)	Cathode Anode	Lowest Operation Temperature (°C)	Specific Capacity (mAh g ^{−1})	Capacity Retention/ Number of Cycles	Ref.
0.8 M NaOTf+0.2 M NaBF ₄ in diglyme	<−60	Na ₃ V ₂ (PO ₄) ₃ Na	−40	—	−/80 0.2 C	[74]
0.5 M NaOTf-DEGDME/DOL (2:8)	<−150	Na ₃ V ₂ (PO ₄) ₃ Na	−60	40 0.2 C	91%/100 0.2 C	[71]
0.8 M NaOTf-THF ₃ /DME ₁ (3:1 vol)	—	NaTi ₂ (PO ₄) ₃ Na	−20	88.8 1 C	96.28%/1000 1C	[78]
1 M NaPF ₆ in THF	—	HC Na	−20	181 2 A g ^{−1}	95%/1000 2 A g ^{−1}	[72]
0.5 M NaPF ₆ in diglyme	—	Na ₃ V ₂ (PO ₄) ₂ F ₃ Na	−20/−60	−60°C 79.2 0.2 C	−20°C 95.58%/1000 10C	[79]
0.3 M NaPF ₆ in diglyme/THF	<−40	Na ₃ V ₂ (PO ₄) ₃ Na	−20	80 0.5 C	−/250 0.5 C	[80]
1 M NaPF ₆ dissolved in diglyme	−71.2	Na ₄ Fe ₃ (PO ₄) ₂ P ₂ O ₇ @C Bi	−40/−60	−60°C 257 20 mA g ^{−1}	100%/40 200 mA g ^{−1}	[27]
0.5 M NaPF ₆ in diglyme	<−70	PTPAn artificial graphite	−70	61 0.01 A g ^{−1}	—	[26]

Overall, ether-based solvents commonly have lower freezing points, which allows the electrolyte to remain in a liquid state and high ionic conductivity at lower temperatures. Moreover, ether-based electrolytes are relatively stable for SMA. However, they are prone to be oxidized decomposition, and their limited high-voltage stability restricts their wider application.

Ionic Liquid Electrolytes

As mentioned above, the nature of solvents is the main reason that affects the LT performances of the electrolytes of SIBs. Therefore, whether solvent-free ionic liquid electrolyte can become a potential candidate for LT electrolyte of SIB is a direction worth exploring. As we know, it is unrealistic for common sodium salts to be used directly as ionic liquids, because their melting point is usually much higher than RT. Therefore, the main design idea of solvent-free LT ionic liquid electrolyte is that dissociate sodium salt by selecting ionic liquid with freezing point far below room temperature as "solvent". Huang et al.^[81] demonstrated that the 1.0 M

Na[FSA]-[C₃C₁pyrr][FSA](C₃C₁pyrr⁺=N-methyl-N-propylpyrrolidiny) electrolyte could be used as LT electrolyte for SIBs. Thanks to the slow increase of charge-transfer resistance in above electrolyte as the temperature decreases (Figure 4a and 4b), the Na₃V₂(PO₄)₂F₃@C cathode with above electrolyte had a favorable electrochemical performance within a wide temperature range, which achieved the reversible capacities of 102.4 mAh g^{−1} and 51.3 mAh g^{−1} at 0 °C and −20 °C, respectively (Figure 4c). In addition, the LT electrochemical properties of NaNTf₂-C₄mpyrNTf₂(1-butyl-1-methylpyrrolidinium bis (trifluoromethylsulfonyl) amide) and NaFSI-P_{111i4}FSI (trimethyl iso-butyl phosphonium bis (fluorosulfonyl)imide) have also been studied^[83,84].

Moreover, the main advantage of ionic liquids in LT applications compared to traditional organic solvents is that their cation-anion structures can be reasonably designed to meet different requirements, thus achieving specific physicochemical properties^[85,86], as shown in Table 4. For example, K. Matsumoto et al.^[87] firstly used the ionic liquid to achieve good

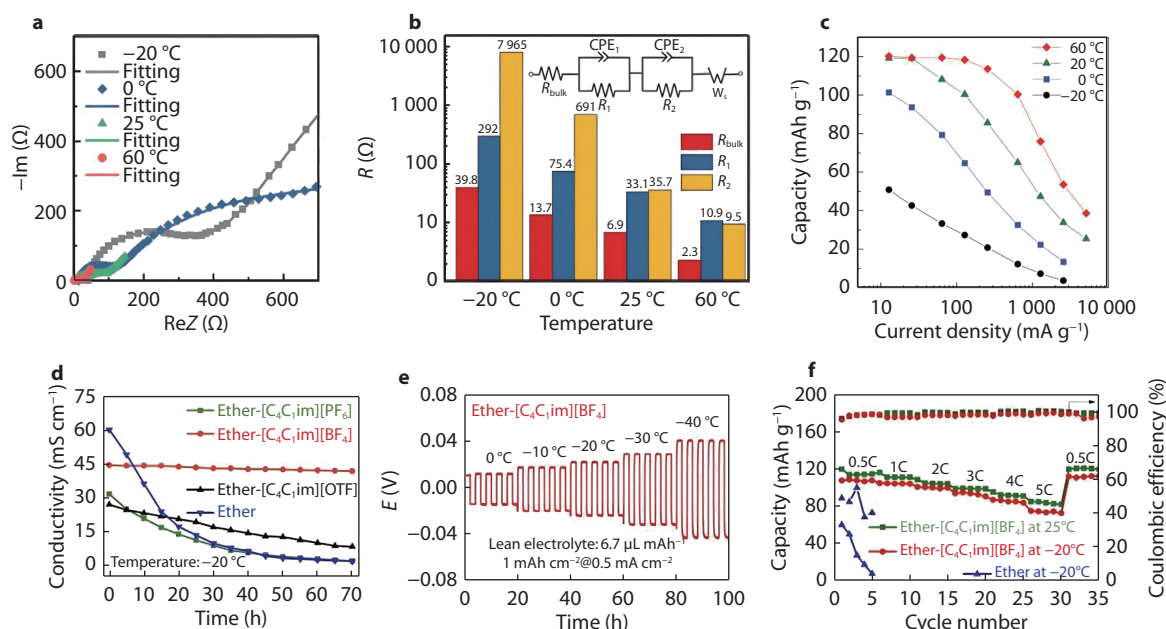


Fig. 4 **a** Nyquist plots and **b** resistances obtained from EIS fitted plots for $\text{Na}_3\text{V}_2(\text{PO}_4)_3/\text{C}$ symmetric cells. **c** Rate performance of $\text{Na}_3\text{V}_2(\text{PO}_4)_3/\text{C} \parallel \text{Na}$ cells from $-20\text{ }^\circ\text{C}$ to $60\text{ }^\circ\text{C}$.^[81] Copyright 2020, Wiley-VCH. **d** Ionic conductivity of different electrolytes changes from $-20\text{ }^\circ\text{C}$ to $25\text{ }^\circ\text{C}$. **e** Temperature-dependent galvanostatic cycling of $\text{Na} \parallel \text{Na}$ symmetric cells with a cycling capacity of 1 mAh cm^{-2} at 0.5 mA cm^{-2} . **f** Rate performance of $\text{Na}_3\text{V}_2(\text{PO}_4)_3 \parallel \text{Na}$ cells with different electrolytes at $25\text{ }^\circ\text{C}$ and $-20\text{ }^\circ\text{C}$.^[82] Copyright 2020, Wiley-VCH.

Table 4. The comparison of LT performance of ionic liquid electrolytes for SIBs.

Electrolytes	Freezing Point ($^\circ\text{C}$)	Cathode Anode	Lowest Operation Temperature ($^\circ\text{C}$)	Specific Capacity (mAh g^{-1})	Capacity Retention/ Number of Cycles	Ref.
1 M Na[FSA]-[C ₃ C ₁ pyrr][FSA]	—	$\text{Na}_3\text{V}_2(\text{PO}_4)_3/\text{C} \parallel \text{Na}$	0	102.4 0.1 C	—/50 0.1 C	[81]
0.1 M NaTf ₂ -C ₄ mpyrNTf ₂ with 5 wt% SiO ₂	T _g -85	—	—	—	—	[83]
2.3 M NaFSI in P ₁₁₁₁₄ FSI	-71	—	—	—	—	[84]
1 M NaPF ₆ in [C ₄ C ₁ im][BF ₄] and diglyme	<-40	$\text{Na}_3\text{V}_2(\text{PO}_4)_3 \parallel \text{Na}$	-20	112.9 0.5 C	95.3%/500 3 C	[82]
Na[FSA]-[C ₂ C ₁ im][FSA] (3:7 mol)	—	Na Cu (first attempt)	0	—	—/18 0.06 mAh cm ⁻²	[87]

SMA compatibility. Specifically, the Na deposition/dissolution in the Na[FSA]-[C₂C₁im][FSA] (C₂C₁im⁺=1-ethyl-3-methylimidazolium) ionic liquid electrolyte exhibited a reversible capacity of 0.06 mAh cm^{-2} at 1 mA cm^{-2} at $0\text{ }^\circ\text{C}$. Although there is no effect of solvent, the high viscosity of ionic liquid at LT also limits its application. To this end, Hu et al.^[82] presented an optimized ether-ionic liquid composite electrolyte, which maintained a high ionic conductivity at $-20\text{ }^\circ\text{C}$ (Figure 4d) and had good compatibility with SMA even at $-40\text{ }^\circ\text{C}$ (Figure 4e). The $\text{Na}_3\text{V}_2(\text{PO}_4)_3$ cathode with 1.0 M NaPF_6 in [C₄C₁im][BF₄]/diglyme electrolyte could deliver a reversible capacity of 112.9 mAh g^{-1} at $-20\text{ }^\circ\text{C}$ (Figure 4f).

In sum, the properties of ionic liquid electrolytes depend on the type of cation and anion present. However, the low ionic conductivity, toxicity and high cost of ionic liquids limit their widespread application.

Aqueous Electrolytes

Fundamental of LT Aqueous Electrolyte

Compared to organic electrolytes, aqueous electrolytes have the merits of high safety, ionic conductivity, environmental concerns, and low cost, thus attracting tremendous

attention in recent years.^[88–90] However, conventional aqueous electrolytes also have the problems of narrow electrochemical stability windows (ESW) and inherent high freezing points, which severely restricts the application of aqueous electrolytes under subzero temperatures.^[32,91] When liquid water transforms into ice, it forms long-range order structures due to the enhancement of hydrogen bonds (HBs) between water molecules.^[92–94] As for the aqueous electrolytes of SIBs, their charge-carrier ions and main-solvents are fixed. Therefore, the core of LT aqueous electrolyte design is to prevent the freezing of water to ice.^[95] In the case of aqueous electrolytes, in 2019, the high-concentration electrolytes were started to be utilized to improve the LT performances of SIBs due to their low freezing points.^[96,97] However, at lower temperatures, high-concentration electrolytes will inevitably result in the precipitation of sodium salts, leading to the increase of viscosity and reduction of ionic conductivity. In the same year, the new strategy emerged that constructing mixed solvents of organic and aqueous solutions.^[98–100] Some latest studies have also combined above two strategies to optimize the LT-performances for SIBs. All these strategies essentially aim to reduce the freezing point of aqueous electrolytes by destroying the original HB network among water

molecules. However, there are substantial difference between them, which will be described in detail in the next section.

Advances in developing in LT Aqueous Electrolyte

High-concentration Electrolytes

In fact, the freezing point of the aqueous electrolyte de-

pends on its concentration. When sodium salt dissolves in water to form electrolyte, the freezing point of electrolyte is far lower than that of pure water. For example, even for the conventional-concentration aqueous electrolyte of 2 M NaClO_4 , it has good LT performance.^[101] Although the full cell $(\text{Ni}(\text{OH})_2 \parallel \text{NaTi}_2(\text{PO}_4)_3\text{@C})$ with 2 M NaClO_4 aqueous electrolyte exhib-

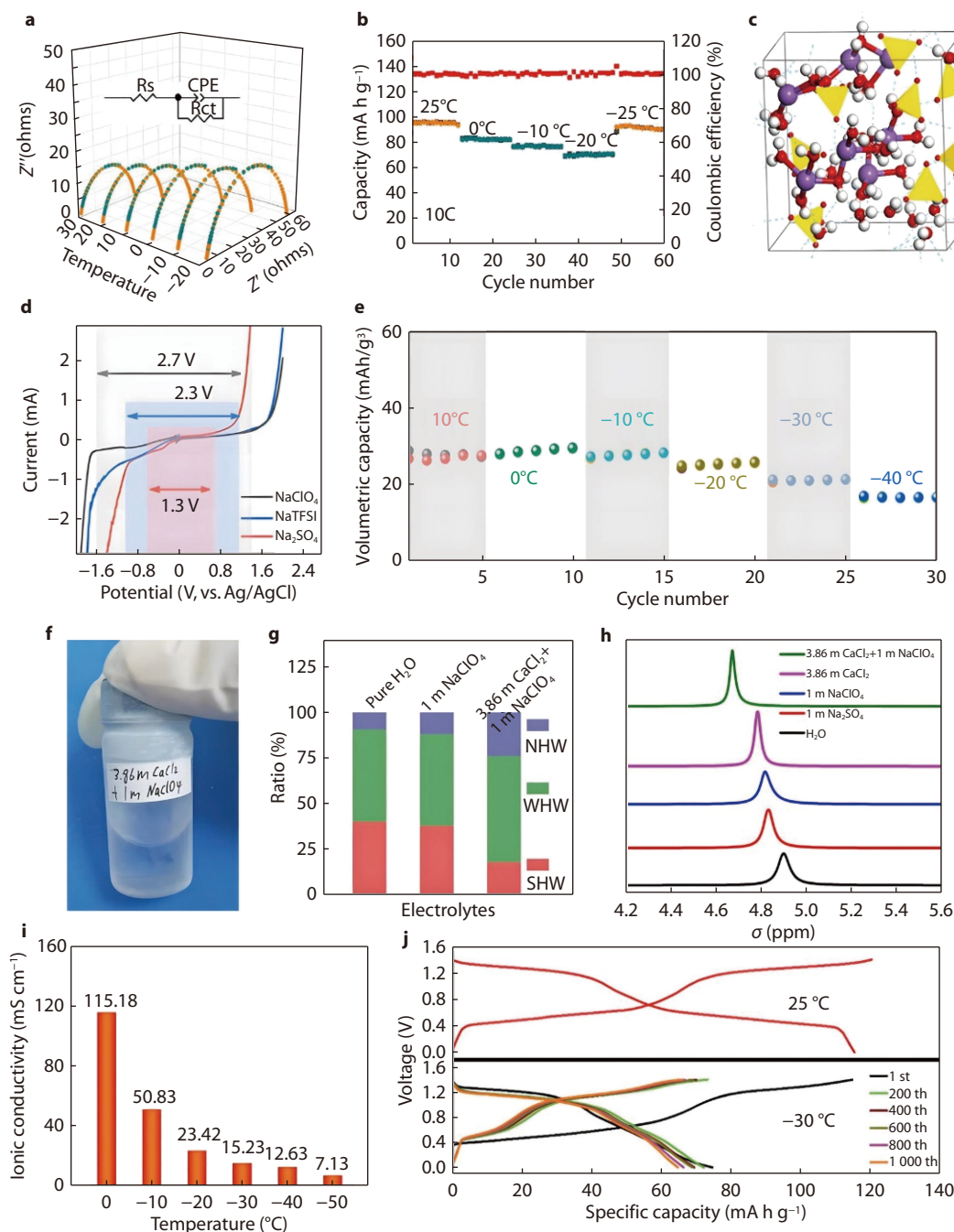


Fig. 5 **a** Fitting map of the Nyquist plots and equivalent circuit for $\text{Ni}(\text{OH})_2 \parallel \text{NaTi}_2(\text{PO}_4)_3\text{@C}$ cells at different temperatures. **b** Cycle test of $\text{Ni}(\text{OH})_2 \parallel \text{NaTi}_2(\text{PO}_4)_3\text{@C}$ cells at different temperatures at 10 °C.^[101] Copyright 2019, American Chemical Society. **c** 17 M NaClO_4 electrolyte conducted by MD simulations. **d** ESW of 17 M NaClO_4 , 8.4 M NaTFSI and 1.3 M Na_2SO_4 electrolyte. **e** Cycle test of $\text{Na}_3\text{V}_2(\text{PO}_4)_3$ symmetric cells at different temperatures at 0.3 mA cm^{-2} .^[102] Copyright 2021, Elsevier. **f** Optical photograph of 3.86 m CaCl_2 + 1 m NaClO_4 electrolyte at -50°C . **g** The component proportions of water with different hydrogen bond for various electrolytes. **h** ^1H NMR results for different electrolytes. **i** Ionic conductivity of 3.86 m CaCl_2 + 1 m NaClO_4 electrolyte changes from -50°C to 0°C . **j** Charge/discharge curves of $\text{Na}_2\text{CoFe}(\text{CN})_6 \parallel$ active carbon cells at -30°C and 25°C .^[103] Copyright 2022, Wiley-VCH.

ited an increase of resistance with the temperature decrease (Figure 5a), it still exhibited a high RT capacity retention (Figure 5b) and a high capacity retention of 85% at -20°C after 10000 cycles at 10°C . This is because the dissolution of sodium salt in water is actually a formation process of strong interaction between Na^{+} and water molecules, which can destroy the HB network between water molecules and inhibit ice formation. However, the ESW of dilute electrolyte is too narrow to match high-voltage electrode materials. And its limited LT operating range still cannot meet the actual demand. To this end, Wang et al.^[102] had further researched the LT performance of 17 M NaClO_4 aqueous electrolyte. As shown in Figure 5c, molecular dynamics (MD) simulations revealed the structure of above high-concentration electrolyte had strong ion-water interactions, theoretically. This led a relatively wide ESW, which matched well with $\text{Na}_3\text{V}_2(\text{PO}_4)_3$ electrode (Figure 5d). Synergistic with the excellent LT properties of above electrolyte, the $\text{Na}_3\text{V}_2(\text{PO}_4)_3 \parallel \text{Na}_3\text{V}_2(\text{PO}_4)_3$ symmetric cell with 17 M NaClO_4 as electrolyte displayed a capacity of 16 mAh cm^{-3} at 10°C under -40°C and 88% RT capacity retention (Figure 5e). Similarly, it had also been proved that the high-concentration 10 M NaClO_4 –0.17 M $\text{Zn}(\text{CH}_3\text{COO})_2$ electrolyte could achieve both wide ESW (about 2.5 V) and low freezing point, because the ion-water interactions effectively reduce the activity of water and paly a “structure-breaking” effect on the HB network of water.^[104] Moreover, after introducing the SEI film-forming additive of Vinylene carbonate (VC), the $\text{Na}_3\text{V}_2(\text{PO}_4)_3 \parallel \text{Zn}$ hybrid battery exhibited a specific discharge capacity of 90 mAh g^{-1} at 0.2 A g^{-1} under -20°C . Interestingly, Reber et al.^[105] found that utilizing asymmetric anions in high-concentration electrolytes could also suppress their crystallization. However, how the anions asymmetry influences the HB network and electrolyte’s structure was not clearly elucidated in this study. Inspired by the research of LT aqueous zinc batteries, the influence of different anions on the tetrahedral entropy of water molecules in an electrolyte

varies, thereby affecting the freezing point of the electrolyte.^[106] Compared to other anions, ClO_4^{-} causes a higher tetrahedral entropy of water molecules, making it difficult to form a continuous hydrogen bonding network. This, in turn, lead to a decrease in the electrolyte’s freezing point.

Nevertheless, due to the high salt concentration, the LT electrochemical performance of high-concentration electrolytes is still hindered by the increased viscosity and reduced ionic conductivity. Therefore, Zhu and coworkers^[103] firstly introduced an inert inorganic anti-freezing additive of CaCl_2 into 1 m NaClO_4 electrolyte for LT-SIBs (Figure 5f). The CaCl_2 decreased strong hydrogen bonding water content in the aqueous electrolyte significantly and destroyed the pristine HB network, resulting in reducing the freezing point of electrolyte (Figure 5g and 5h). Consequently, at -50°C , the optimized electrolyte still exhibits high ionic conductivity of 7.13 mS cm^{-1} (Figure 5i). Then, the $\text{Na}_2\text{CoFe}(\text{CN})_6 \parallel$ active carbon full cell using 3.86 m CaCl_2 +1 m NaClO_4 aqueous electrolyte displayed a discharge specific capacity of 74.5 mAh g^{-1} at 1°C at -30°C (Figure 5j). In addition, as shown in Table 5, sodium dodecyl sulfate^[107] has also been proved to essentially damage the pristine HB network of water through ion-water interaction, thus resulting in the expanded ESW and reduced freezing point.

Hybrid Electrolytes

Different with that the high-concentration electrolyte reduce the freezing point through the ion-water interaction, the cosolvents-water hybrid electrolytes destroy the original HB network by constructing the inter-molecular HB between the cosolvents and water. Havemeyer^[110] firstly found that the freezing point of dimethyl sulfoxide (DMSO)–water mixed solvent could be as low as $\sim -140^{\circ}\text{C}$, when DMSO with the molar fraction of 0.3 was added. Then, Nian et al.^[108] further constructed a hybrid electrolyte of 2 M NaClO_4 solution based on the above DMSO–water mixture and demonstrated that

Table 5. The comparison of LT performance of aqueous electrolytes for SIBs.

	Electrolytes	Freezing Point ($^{\circ}\text{C}$)	Cathode Anode	Lowest operation temperature ($^{\circ}\text{C}$)	Specific Capacity (mAh/g)	Capacity Retention/ Number of Cycles	Ref.
High-concentration Electrolytes	2 M NaClO_4	–	$\text{Ni}(\text{OH})_2 \parallel \text{NaTi}_2(\text{PO}_4)_3 @ \text{C}$	-20	–	85%/10000 10 C	[101]
	17 M NaClO_4 SiO ₂ (0.5 g/6 mL)	-50	$\text{Na}_3\text{V}_2(\text{PO}_4)_3 \parallel \text{Na}_3\text{V}_2(\text{PO}_4)_3$	$-15/-40$	-40°C 16 mAh cm^{-3} 0.3 mA cm^{-2}	-15°C 91%/6000.3 mA cm^{-2}	[102]
	10 M NaClO_4 –0.17 M $\text{Zn}(\text{CH}_3\text{COO})_2$ –2 wt% VC	<-30	$\text{Na}_3\text{V}_2(\text{PO}_4)_3 \parallel \text{Zn}$	$-10/-20$	-20°C 90 0.2 A g^{-1}	-10°C 92%/400 0.2 A g^{-1}	[104]
	25 m NaFSI + 10 m NaTFSI	<-40	$\text{Na}_3(\text{VOPO}_4)_2\text{F} \parallel \text{NaTi}_2(\text{PO}_4)_3$	-10	65 0.2 C	74%/500 0.2 C	[105]
	3.86 m CaCl_2 +1 m NaClO_4 solution	<-50	$\text{Na}_2\text{CoFe}(\text{CN})_6 \parallel$ active carbon	-30	74.5 1 C	86.7%/1000 1 C	[103]
	0.5 M Li_2SO_4 –0.5 M Na_2SO_4 with 756 mM SDS	–	$\text{NaTi}_2(\text{PO}_4)_3 \parallel \text{LiMn}_2\text{O}_4$	-15	–	71.3%/1000 1 C	[107]
Hybrid Electrolytes	2 M NaClO_4 solution with DMSO (30% mole)	<-130	active carbon $\text{NaTi}_2(\text{PO}_4)_3 @ \text{C}$	-50	68 0.5 C	$-/100$ 0.5 C	[108]
	1 M Na_2SO_4 +50 mL MA–SiO ₂ (15 g/100 mL)	–	active carbon $\text{NaTi}_2(\text{PO}_4)_3 @ \text{C}$	-30	61.8 0.13 A g^{-1}	–	[61]
	1 m NaNO_3 glycerol–water (2:1 wt)	<-80	$\text{Ni}_2\text{ZnHCF} \parallel \text{PTCDI}$	-10	40 100 mA g^{-1}	$-/300$ 100 mA g^{-1}	[111]
	2 M NaNO_3 /66.7 wt% sucrose (or 60.0 wt% maltose/66.7 wt% D-fructose)	<-50	–	–	–	–	[112]
	1 M sodium acetate in ethanol/water (5:1 vol)	–	$\text{Na}_{0.44}\text{MnO}_2 \parallel \text{Zn}$	0	–	94%/50 50 mA g^{-1}	[113]
	2 m NaTFSI/PEGMA–BEMA+FEC with 10wt% H ₂ O	<-25	$\text{Na}_{2/3}\text{Mn}_{2/3}\text{Co}_{1/3}\text{O}_{1.98}\text{F}_{0.02} \parallel \text{HC}$	-25	32 0.2 A g^{-1}	–	[114]
	17 m NaClO_4 –H ₂ O/FA (3:7 vol)	<-50	active carbon PNTCDA	-50	78.58 1 C	100%/8000 4 C	[109]

strong HBs between S=O of DMSO and O-H of water were stably formed in above hybrid electrolyte, which could destroy the HB network within water molecules, resulting in the decrease of the freezing point (Figure 6a and 6b). The temperature-dependent ionic conductivity of 2 M solutions of NaClO₄ in pure water, DMSO-water mixture, and pure DMSO was shown in Figure 6c, the hybrid electrolyte exhibited the highest ionic conductivity of 0.11 mS cm⁻¹ at -50 °C. Mean-

while, it did have a low freezing point of -130 °C (Figure 6d). The active carbon || NaTi₂(PO₄)₃@C full cell using above electrolyte exhibited a capacity of 68 mAh g⁻¹ at 0.5 C at -50 °C (Figure 6e). Subsequently, Cheng et al.^[61] selected methyl alcohol (MA) as the anti-freezing cosolvent of the electrolyte for LT-SIBs. The specific capacity of active carbon || NaTi₂(PO₄)₃@C full batteries using the 1.0 M Na₂SO₄ in water-MA (2:1 by vol) hydrogel electrolyte could reach 61.8 mAh g⁻¹

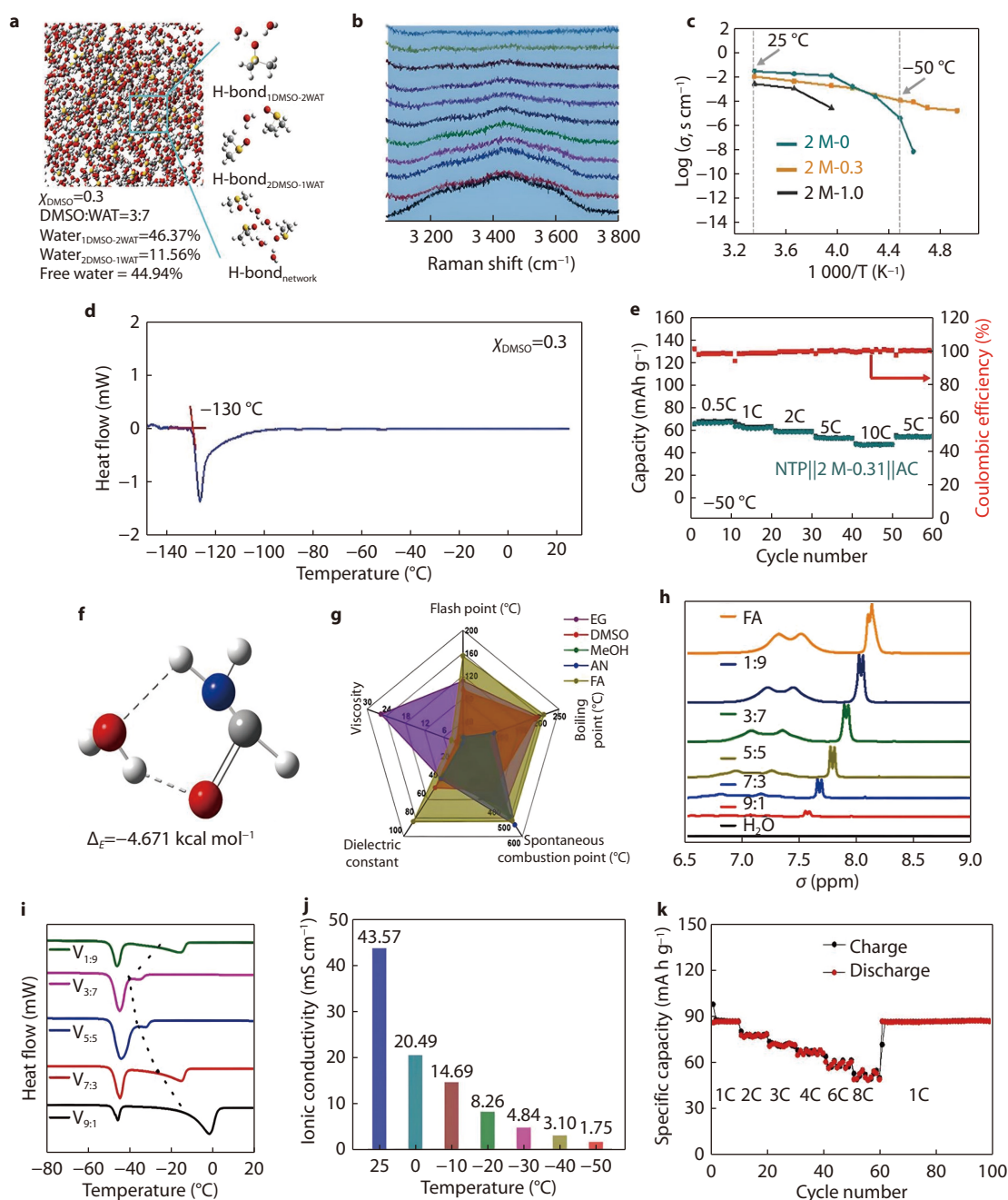


Fig. 6 **a** Conformation analysis of DMSO-water mixture conducted by MD simulations. **b** Raman spectra of DMSO-water mixtures with different molar fractions of DMSO. **c** Temperature-dependent ionic conductivity of different electrolytes. **d** Heat flow of hybrid electrolyte. **e** Rate performance of active carbon || NaTi₂(PO₄)₃@C cell at 0.5 C at -50 °C.^[108] Copyright 2019, Wiley-VCH. **f** Intermolecular interaction among H₂O-FA clusters conducted by DFT calculations. **g** Comparison of the physicochemical properties for different organic cosolvents. **h** ¹H NMR results and **i** heat flow of FA/water mixtures with different volume ratio of FA. **j** Ionic conductivity of hybrid electrolyte changes from -50 °C to 25 °C. **k** Rate performance of active carbon || PNTCDA cell from 1 to 8 C at -50 °C.^[109] Copyright 2022, Elsevier.

at 1 C under -30°C , meaning 65.05% of that at 25°C . Similar hydroxyl-containing compounds, as shown in Table 5, such as glycerol^[111], hydroxyl-rich sugars (maltose, sucrose, and D-fructose with rich hydroxyl groups)^[112] and ethanol^[113], were also used in LT electrolytes for SIBs. Within a temperature range of -50°C to 80°C , 2 M NaNO_3 electrolytes with 66.7 wt% sucrose/D-fructose or 60 wt% maltose exhibited almost none heat fluctuations in heat flow value, which confirms the effect of hydroxyl-containing compounds in reducing the freezing point of electrolytes. Moreover, the ESWs and ionic conductivities of above electrolytes (2 M NaNO_3 /60.0 wt% maltose: $\sim 2.392\text{ V}$, 8.536 mS cm^{-1} ; 2 M NaNO_3 /66.7 wt% D-fructose: $\sim 2.600\text{ V}$, 3.812 mS cm^{-1} ; 2 M NaNO_3 /66.7 wt% sucrose: $\sim 2.812\text{ V}$, 3.376 mS cm^{-1}) are all higher than that of the 2 M NaNO_3 electrolyte (1.652 V). Besides, hydroxyl-containing polymers are also used in the development of LT electrolytes for SIBs. For example, Rong et al.^[114] have demonstrated that the $\text{Na}_{2/3}\text{Mn}_{2/3}\text{Co}_{1/3}\text{O}_{1.98}\text{F}_{0.02} \parallel \text{HC}$ full cell exhibited an initial discharge capacity of 32 mAh g^{-1} at 0.2 A g^{-1} under -25°C by using a hybrid electrolyte contains 10% water, 2 M NaTFSI and polymer matrix consists of poly(ethylene glycol) methyl ether methacrylate (PEGMA) and bisphenol A ethoxylate dimethacrylate (BEMA).

Recently, 17 m NaClO_4 LT aqueous electrolyte was developed by introducing a strong polar solvent formamide (FA)^[109], which is a complex design strategy combining ion-water interaction with cosolvent-water interaction (Figure 6f). Compared to other commonly used organic cosolvents, FA has more excellent physicochemical properties as shown in Figure 6g, resulting in being chosen as the solvent of electrolyte for LT-SIBs. In addition, FA molecule possesses both the H-bond acceptor carbonyl groups and donor amino groups, and has more coordination sites than water, so it can form inter-molecular HBs with water more effectively. According to the MD calculations, when the volume ratio of water and FA was 3:7, the stable water-FA clusters could spontaneously form accompanied by the reconstruction of HB network (Figure 6f and 6h). As a result, the above mixed solvent exhibited lowest freezing point among all the solutions and the hybrid electrolyte based on above mixture maintained sufficient ionic conductivity at LT (Figure 6i and 6j). Consequently, as shown in Figure 6k, the active carbon \parallel PNTCDA full cell fabricated with optimized $(\text{NaClO}_4)_{1.7}(\text{H}_2\text{O})_{5.5}(\text{FA})_{5.81}$ electrolyte could still deliver a high specific capacity of 51.07 mAh g^{-1} at 8 C at -50°C (58.5% of the capacity of 1 C).

All in all, aqueous electrolytes are remarkably cost-effective, environmentally friendly, and offer higher safety standards. Nonetheless, aqueous electrolytes commonly exhibit high reactivity, especially at low potentials, where hydrogen evolution reactions are prone to occur, resulting in a narrow ESW.

Summary and Outlook

In summary, the design of electrolyte is effective for improving the LT performance of SIBs, which is expected to play a key role in further promoting the practicality of SIBs in the future. This review clearly points out the main reasons limited the LT performance of SIBs is that the low ionic conductivity and high desolvation energy of organic electrolytes, and

looks forward to the design direction of ideal LT organic electrolyte in theory. The advances of LT organic electrolyte of SIBs are systematically introduced from ester, ether and ionic liquid-based electrolytes, involving various strategies including multiple mixing, EC-free, weakly solvated and solvent-free. Then, by analyzing the mechanism of water freezing, this review proposed that destroying and reconstruction of hydrogen bond network among water at LT is the main design idea for inhibiting the freezing of aqueous electrolyte and alleviating the LT failure of aqueous SIBs. From the two internal mechanisms of ion-water and cosolvent-water interactions, the research progress of two typical LT aqueous electrolytes, such as high-concentration and hybrid electrolytes, are summarized, comprehensively. Different types of electrolytes have their unique advantages, and they need to be matched with appropriate electrode materials to better exploit their performance. Further optimization of the shortcomings of above electrolytes is the key to improving LT performance of SIBs. It is foreseeable that ether-based electrolytes after solving the problem of high-voltage oxidation stability and the aqueous electrolytes with wider ESWs are the most promising choices for LT-SIBs. Although certain development achievements have been made, the design of the electrolyte for LT-SIBs still focuses more on the regulation of the electrolyte formula, while the mechanism research and other aspects lack sufficient research depth. Here, some perspectives and prospects for future research on LT-SIBs are presented.

1). The variation of interactions between the components in the electrolyte with the temperature fluctuation is noteworthy. Ion-ion, ion-solvent, and solvent-solvent interactions are the key factors determining the properties of electrolytes. Both the construction of weakly solvating electrolytes and the destruction of HB network in aqueous electrolytes depend on the regulation of the interaction strength of each component in the electrolyte. Therefore, the characterization and study of these interactions may deepen our fundamental understanding of the electrolytes for LT-SIBs.

2). Ion transport in the bulk electrolyte and the electrode/electrolyte interface is the main factor determining the performance of LT-SIBs. At LT, the ionic conductivity of the electrolyte decreases, and the ion desolvation process becomes the rate-controlling step of ion transport, which seriously affects the rate of SIBs. Through the combination of theoretical calculations and experiments, an in-depth understanding of the ion transport mechanism can be beneficial to guide the design of electrolytes for LT-SIBs.

3). High-entropy electrolytes are emerging as a promising direction for the development of LT electrolytes in SIBs.^[115] The design concept of high-entropy electrolytes is to select multiple solvents or salts with complementary properties to optimize the comprehensive performance of the electrolyte.^[116] The application of high-entropy strategy in SIBs also needs to consider the strength of interactions between Na^+ -solvents and Na^+ -anions, to achieve a diverse and balanced solvation structure. In addition, combining appropriate components can enhance the thermodynamic stability and entropy of the electrolyte, thereby ensuring the ion transport properties of the electrolyte and reducing its freezing point.

4). The collaborative design of electrolytes and electrode

materials will further improve the performance of LT-SIBs. The behavior of the solvated Na⁺ at the interface is closely related to the electrode material. Dual-ion batteries with eliminating the desolvation process and alloying reactions such as Na-Bi/Na-Sn jointly demonstrate the effectiveness of the co-design of electrolytes and electrode materials. Meanwhile, compared with artificial SEI films, it is a more effective and economical strategy to in situ construct SEI/CEI films by selecting appropriate electrolytes and electrode materials.

5). Advanced in situ characterization techniques and theoretical calculations are conducive to clearly revealing the reaction mechanism inside LT-SIBs. In situ characterization techniques are necessary to unveil the transport mechanism of charge-carrier ions, ion desolvation process, interfacial reaction and other processes. In addition, machine learning and theoretical calculations such as MD and density functional theory (DFT) can effectively predict the physicochemical properties of electrolytes and the compatibility of electrolytes and electrode materials.

■ ACKNOWLEDGEMENTS

The authors thank the support from the National Key R&D Program of China (No. 2021YFA1202300), the National Natural Science Foundation of China (No. 22075132 and 22209069), the Natural Science Foundation of Jiangsu Province, China (No. BK20211556 and BK20220783), Jiangsu Province Carbon Peak and Neutrality Innovation Program (Industry tackling on prospect and key technology, No. BE2022002-2), the Shenzhen Science and Technology Innovation Committee (No. RCYX20200714114524165 and JCYJ20210324123002008), and Guangdong Basic and Applied Basic Research Foundation (2022A1515010026). We also thank Fundamental Research Funds for the Central Universities and Frontiers Science Cent for Critical Earth Material Cycling Fund.

■ AUTHOR'S CONTRIBUTION

Tianze Shi wrote the draft; Ruilin Hou and Shaohua Guo edited and polished the paper. All authors had approved the final version.

■ CONFLICT OF INTEREST

The authors declare no conflict of interest.

■ REFERENCES

1. H.-Y. Lu, R.-L. Hou, S.-Y. Chu, H.-S. Zhou, S.-H. Guo, *Acta Phys. Chim. Sin.*, 2023, 39, 2211057
2. J.-Y. Hwang, S.-T. Myung, Y.-K. Sun, *Chem. Soc. Rev.*, 2017, 46, 3529
3. Q. Wang, Y. Liao, X. Jin, C. Cheng, S. Chu, C. Sheng, L. Zhang, B. Hu, S. Guo, H. Zhou, *Angew. Chem. Int. Ed.*, 2022, 61, e202206625
4. S. Chu, C. Zhang, H. Xu, S. Guo, P. Wang, H. Zhou, *Angew. Chem.*, 2021, 133, 13478
5. H. Xu, C. Cheng, S. Chu, X. Zhang, J. Wu, L. Zhang, S. Guo, H. Zhou, *Adv. Funct. Mater.*, 2020, 30, 2005164
6. X. Zhu, L. Wang, *EcoMat*, 2020, 2, e12043
7. Z. Na, W. Feng, W. Chuan, B. Ying, L. Yitong, *Energy Storage Science and Technology*, 2016, 5, 285.
8. Y. You, H.-R. Yao, S. Xin, Y.-X. Yin, T.-T. Zuo, C.-P. Yang, Y.-G. Guo, Y. Cui, L.-J. Wan, J. B. Goodenough, *Adv. Mater.*, 2016, 28, 7243
9. A. Gupta, A. Manthiram, *Adv. Energy Mater.*, 2020, 10, 2001972
10. P. Mei, Y. Zhang, W. Zhang, *Nanoscale*, 2023, 15, 987
11. A. Hu, F. Li, W. Chen, T. Lei, Y. Li, Y. Fan, M. He, F. Wang, M. Zhou, Y. Hu, *Adv. Energy Mater.*, 2022, 12, 2202432
12. Y.-J. Fang, Z.-X. Chen, X.-P. Ai, H.-X. Yang, Y.-L. Cao, *Acta Phys. Chim. Sin.*, 2017, 33, 211
13. P. Chen, C. Wu, Z. Wang, S. Li, X. Xu, J. Tu, Y.-L. Ding, *ACS Appl. Energy Mater.*, 2022, 5, 2542
14. H. Zhang, J. Song, J. Li, J. Feng, Y. Ma, L. Ma, H. Liu, Y. Qin, X. Zhao, F. Wang, *ACS Appl. Mater. Interfaces*, 2022, 14, 16300
15. X. Rui, X. Zhang, S. Xu, H. Tan, Y. Jiang, L. Y. Gan, Y. Feng, C. C. Li, Y. Yu, *Adv. Funct. Mater.*, 2021, 31, 2009458
16. Z. Bai, X. Lv, D.-H. Liu, D. Dai, J. Gu, L. Yang, Z. Chen, *ChemElectroChem*, 2020, 7, 3616
17. H.-H. Fan, H.-H. Li, Z.-W. Wang, W.-L. Li, J.-Z. Guo, C.-Y. Fan, H.-Z. Sun, X.-L. Wu, J.-P. Zhang, *ACS Appl. Mater. Interfaces*, 2019, 11, 47886
18. Y.-Y. Wang, B.-H. Hou, J.-Z. Guo, Q.-L. Ning, W.-L. Pang, J. Wang, C.-L. Lü, X.-L. Wu, *Adv. Energy Mater.*, 2018, 8, 1703252
19. J.-Y. Hwang, S.-M. Oh, S.-T. Myung, K. Y. Chung, I. Belharouak, Y.-K. Sun, *Nat. Commun.*, 2015, 6, 6865
20. S. Yuan, W. Zhao, Z. Zeng, Y. Dong, F. Jiang, L. Wang, Y. Yang, J. Zhu, X. Ji, P. Ge, *J. Mater. Chem. A*, 2022, 10, 22645
21. Y. Cao, X. Cao, X. Dong, X. Zhang, J. Xu, N. Wang, Y. Yang, C. Wang, Y. Liu, Y. Xia, *Adv. Funct. Mater.*, 2021, 31, 2102856
22. B. Liu, Q. Zhang, L. Li, L. Zhang, Z. Jin, C. Wang, Z. Su, *Chem. Eng. J.*, 2021, 405, 126689
23. M. Nowak, W. Zajac, J. Molenda, *Energy*, 2022, 239, 122388
24. Q. Shi, R. Qi, X. Feng, J. Wang, Y. Li, Z. Yao, X. Wang, Q. Li, X. Lu, J. Zhang, Y. Zhao, *Nat. Commun.*, 2022, 13, 3205
25. Y. Xia, L. Que, F. Yu, L. Deng, Z. Liang, Y. Jiang, M. Sun, L. Zhao, Z. Wang, *Nano-Micro Lett.*, 2022, 14, 143
26. J. Chen, Y. Peng, Y. Yin, Z. Fang, Y. Cao, Y. Wang, X. Dong, Y. Xia, *Angew. Chem. Int. Ed.*, 2021, 60, 23858
27. Z. Li, Y. Zhang, J. Zhang, Y. Cao, J. Chen, H. Liu, Y. Wang, *Angew. Chem. Int. Ed.*, 2022, 61, e202116930
28. F. Mo, Z. Lian, B. Fu, Y. Song, P. Wang, F. Fang, Y.-N. Zhou, S. Peng, D. Sun, *J. Mater. Chem. A*, 2019, 7, 9051
29. T. Yamamoto, T. Nohira, R. Hagiwara, A. Fukunaga, S. Sakai, K. Nitta, *Electrochim. Acta*, 2016, 211, 234
30. W. Liu, P. Liu, D. Mitlin, *Adv. Energy Mater.*, 2020, 10, 2002297
31. H. Lu, X. Chen, Y. Jia, H. Chen, Y. Wang, X. Ai, H. Yang, Y. Cao, *Nano Energy*, 2019, 64, 103903
32. Z. Chen, K. Wang, P. Pei, Y. Zuo, M. Wei, H. Wang, P. Zhang, N. Shang, *Nano Res.*, 2023, 16, 2311
33. M.-L. Xu, M.-C. Liu, Z.-Z. Yang, C. Wu, J.-F. Qian, *Acta Phys. Chim. Sin.*, 2023, 39, 2210043
34. N. Zhang, T. Deng, S. Zhang, C. Wang, L. Chen, C. Wang, X. Fan, *Adv. Mater.*, 2022, 34, e2107899
35. D. Hubble, D. E. Brown, Y. Zhao, C. Fang, J. Lau, B. D. McCloskey, G. Liu, *Energy Environ. Sci.*, 2022, 15, 550
36. J. Huang, X. Dong, N. Wang, Y. Wang, *Curr. Opin. Electrochem.*, 2022, 33, 100949
37. P. Li, N. Hu, J. Wang, S. Wang, W. Deng, *Nanomaterials (Basel)*, 2022, 12, 3529
38. M.-D. Slater, D. Kim, E. Lee, C.-S. Johnson, *Adv. Funct. Mater.*, 2013, 23, 947
39. D. Xiao, L. Zhang, Z. Li, H. Dou, X. Zhang, *Energy Storage Mater.*, 2022, 44, 10
40. G. Ah-Lung, B. Flamme, F. Ghamouss, M. Maréchal, J. Jacquemin, *Chem. Commun.*, 2020, 56, 9830
41. M.-Y. Sun, F.-D. Yu, Y. Xia, L. Deng, Y.-S. Jiang, L.-F. Que, L. Zhao, Z.-B. Wang, *Chem. Eng. J.*, 2022, 430, 132750

42. B. Wen, Z. Deng, P.-C. Tsai, Z.-W. Lebens-Higgins, L.-F. Piper, S.-P. Ong, Y.-M. Chiang, *Nat. Energy*, 2020, 5, 578
43. K. Xu, A. von Cresce, U. Lee, *Langmuir*, 2010, 26, 11538
44. Y. Wang, X. Yang, Z. Zhang, X. Hu, Y. Meng, X. Wang, D. Zhou, H. Liu, B. Li, G. Wang, *eScience*, 2022, 2, 573
45. J. Zhang, D.-W. Wang, W. Lv, S. Zhang, Q. Liang, D. Zheng, F. Kang, Q.-H. Yang, *Energy Environ. Sci.*, 2017, 10, 370
46. J. Holoubek, Y. Yin, M. Li, M. Yu, Y.-S. Meng, P. Liu, Z. Chen, *Angew. Chem. Int. Ed.*, 2019, 131, 19068
47. D. Lin, K. Li, Q. Wang, L. Lyu, B. Li, L. Zhou, *J. Mater. Chem. A*, 2019, 7, 19297
48. H. Che, X. Yang, Y. Yu, C. Pan, H. Wang, Y. Deng, L. Li, Z.-F. Ma, *Green Energy Environ.*, 2021, 6, 212
49. Y.-B. Niu, Y.-X. Yin, Y.-G. Guo, *Small*, 2019, 15, 1900233
50. Y. Jin, Y. Xu, P.-M. Le, T.-D. Vo, Q. Zhou, X. Qi, M.-H. Engelhard, B.-E. Matthews, H. Jia, Z. Nie, *ACS Energy Lett.*, 2020, 5, 3212
51. K. Mukai, T. Inoue, Y. Kato, S. Shirai, *ACS Omega*, 2017, 2, 864
52. L. Wang, B. Wang, G. Liu, T. Liu, T. Gao, D. Wang, *RSC Adv.*, 2016, 6, 70277
53. Q. Li, D. Lu, J. Zheng, S. Jiao, L. Luo, C.-M. Wang, K. Xu, J.-G. Zhang, W. Xu, *ACS Appl. Mater. Interfaces*, 2017, 9, 42761
54. J. Chen, Z. Li, N. Sun, J. Xu, Q. Li, X. Yao, J. Ming, Z. Peng, *ACS Energy Lett.*, 2022, 7, 1594
55. T.-R. Jow, M.-B. Marx, J.-L. Allen, *J. Electrochem. Soc.*, 2012, 159, A604
56. F.-A. Soto, P. Yan, M.-H. Engelhard, A. Marzouk, C. Wang, G. Xu, Z. Chen, K. Amine, J. Liu, V.-L. Sprenkle, *Adv. Mater.*, 2017, 29, 1606860
57. L. Raguette, R. Jorn, *J. Phys. Chem. C*, 2018, 122, 3219
58. Y.-X. Yao, X. Chen, C. Yan, X.-Q. Zhang, W.-L. Cai, J.-Q. Huang, Q. Zhang, *Angew. Chem. Int. Ed.*, 2021, 60, 4090
59. E. Barsoukov, D. Kim, H.-S. Lee, H. Lee, M. Yakovleva, Y. Gao, J.-F. Engel, *Solid State Ionics*, 2003, 161, 19
60. J. Xu, J. Zhang, T.-P. Pollard, Q. Li, S. Tan, S. Hou, H. Wan, F. Chen, H. He, E. Hu, K. Xu, X.-Q. Yang, O. Borodin, C. Wang, *Nature*, 2023, 614, 694
61. Y. Cheng, X. Chi, J. Yang, Y. Liu, *J. Energy Storage*, 2021, 40, 102701
62. X. Liu, X. Zheng, X. Qin, Y. Deng, Y. Dai, T. Zhao, Z. Wang, H. Yang, W. Luo, *Nano Energy*, 2022, 103, 107746
63. L. Deng, K. Goh, F.-D. Yu, Y. Xia, Y.-S. Jiang, W. Ke, Y. Han, L.-F. Que, J. Zhou, Z.-B. Wang, *Energy Storage Mater.*, 2022, 44, 82
64. X. Song, T. Meng, Y. Deng, A. Gao, J. Nan, D. Shu, F. Yi, *Electrochim. Acta*, 2018, 281, 370
65. Q. Hu, M. Yu, J. Liao, Z. Wen, C. Chen, *J. Mater. Chem. A*, 2018, 6, 2365
66. X. Zheng, Z. Gu, J. Fu, H. Wang, X. Ye, L. Huang, X. Liu, X. Wu, W. Luo, Y. Huang, *Energy Environ. Sci.*, 2021, 14, 4936
67. Z. Wang, J. Ni, L. Li, *ACS Energy Lett.*, 2022, 7, 4106
68. H.-J. Liang, Z.-Y. Gu, X.-X. Zhao, J.-Z. Guo, J.-L. Yang, W.-H. Li, B. Li, Z.-M. Liu, Z.-H. Sun, J.-P. Zhang, *Sci. Bull.*, 2022, 67, 1581
69. R. Mogensen, A. Buckel, S. Colbin, R. Younesi, *Chem. Mater.*, 2021, 33, 1130
70. R. Väli, A. Jänes, E. Lust, *J. Electrochem. Soc.*, 2016, 163, A851
71. C. Wang, A.-C. Thenuwara, J. Luo, P.-P. Shetty, M.-T. McDowell, H. Zhu, S. Posada-Perez, H. Xiong, G. Hautier, W. Li, *Nat. Commun.*, 2022, 13, 4934
72. Z. Tang, H. Wang, P.-F. Wu, S.-Y. Zhou, Y.-C. Huang, R. Zhang, D. Sun, Y.-G. Tang, H.-Y. Wang, *Angew. Chem. Int. Ed.*, 2022, 61, e202200475
73. X. Fan, X. Ji, L. Chen, J. Chen, T. Deng, F. Han, J. Yue, N. Piao, R. Wang, X. Zhou, X. Xiao, L. Chen, C. Wang, *Nat. Energy*, 2019, 4, 882
74. A.-C. Thenuwara, P.-P. Shetty, N. Kondekar, C. Wang, W. Li, M.-T. McDowell, *J. Mater. Chem. A*, 2021, 9, 10992
75. J. Holoubek, H. Liu, Z. Wu, Y. Yin, X. Xing, G. Cai, S. Yu, H. Zhou, T.-A. Pascal, Z. Chen, P. Liu, *Nat. Energy*, 2021, 6, 303
76. H.-J. Liang, Z.-Y. Gu, X.-X. Zhao, J.-Z. Guo, J.-L. Yang, W.-H. Li, B. Li, Z.-M. Liu, W.-L. Li, X.-L. Wu, *Angew. Chem. Int. Ed.*, 2021, 60, 26837
77. D.-S. Hall, J. Self, J. Dahn, *J. Phys. Chem. C*, 2015, 119, 22322
78. J. Zhou, Y. Wang, J. Wang, Y. Liu, Y. Li, L. Cheng, Y. Ding, S. Dong, Q. Zhu, M. Tang, Y. Wang, Y. Bi, R. Sun, Z. Wang, H. Wang, *Energy Storage Mater.*, 2022, 50, 47
79. Y.-Q. Zheng, M.-Y. Sun, F.-D. Yu, L. Deng, Y. Xia, Y.-S. Jiang, L.-F. Que, L. Zhao, Z.-B. Wang, *Nano Energy*, 2022, 102, 107693
80. Z. Wang, X. Zheng, X. Liu, Y. Huang, L. Huang, Y. Chen, M. Han, W. Luo, *ACS Appl. Mater. Interfaces*, 2022, 14, 40985
81. J. Hwang, K. Matsumoto, R. Hagiwara, *Adv. Energy Mater.*, 2020, 10, 2001880
82. X. Hu, E. Matios, Y. Zhang, C. Wang, J. Luo, W. Li, *Angew. Chem. Int. Ed.*, 2021, 60, 5978
83. S.-A. Mohd Noor, H. Yoon, M. Forsyth, D.-R. MacFarlane, *Electrochim. Acta*, 2015, 169, 376
84. M. Hilder, P.-C. Howlett, D. Saurel, E. Gonzalo, M. Armand, T. Rojo, D.-R. Macfarlane, M. Forsyth, *J. Power Sources*, 2017, 349, 45
85. T. Rütther, A.-I. Bhatt, A.-S. Best, K.-R. Harris, A.-F. Hollenkamp, *Batteries Supercaps*, 2020, 3, 793
86. W. Zhou, M. Zhang, X. Kong, W. Huang, Q. Zhang, *Adv. Sci.*, 2021, 8, 2004490
87. K. Matsumoto, C.-Y. Chen, T. Kiko, J. Hwang, T. Hosokawa, T. No-hira, R. Hagiwara, *ECS Trans.*, 2016, 75, 139
88. H. Zhang, X. Liu, H. Li, I. Hasa, S. Passerini, *Angew. Chem. Int. Ed.*, 2021, 60, 598
89. F. Wan, J. Zhu, S. Huang, Z. Niu, *Batteries Supercaps*, 2020, 3, 323
90. A. von Wald Cresce, K. Xu, *Carbon Energy*, 2021, 3, 721
91. Y. Wang, H. Wei, Z. Li, X. Zhang, Z. Wei, K. Sun, H. Li, *The Chemical Record*, 2022, 22, e202200132
92. Y. Chen, H.-I. Okur, N. Gomopoulos, C. Macias-Romero, P.-S. Cremer, P.-B. Petersen, G. Tocchi, D.-M. Wilkins, C. Liang, M. Ceriotti, *Sci. Adv.*, 2016, 2, e1501891
93. M. Matsumoto, S. Saito, I. Ohmine, *Nature*, 2002, 416, 409
94. E.-B. Moore, V. Molinero, *Nature*, 2011, 479, 506
95. K. Zhu, Z. Sun, Z. Li, P. Liu, H. Li, L. Jiao, *Adv. Energy Mater.*, 2023, 13, 2203708
96. T. Liang, R. Hou, Q. Dou, H. Zhang, X. Yan, *Adv. Funct. Mater.*, 2020, 31, 2006749
97. M. Amiri, D. Belanger, *ChemSusChem*, 2021, 14, 2487
98. Q. Dou, S. Lei, D.-W. Wang, Q. Zhang, D. Xiao, H. Guo, A. Wang, H. Yang, Y. Li, S. Shi, *Energy Environ. Sci.*, 2018, 11, 3212
99. F. Wang, L. Suo, Y. Liang, C. Yang, F. Han, T. Gao, W. Sun, C. Wang, *Adv. Energy Mater.*, 2017, 7, 1600922
100. K. Zhu, Z. Sun, T. Jin, X. Chen, Y. Si, H. Li, L. Jiao, *Batteries Supercaps*, 2022, 5, e202200308
101. Q. Nian, S. Liu, J. Liu, Q. Zhang, J. Shi, C. Liu, R. Wang, Z. Tao, J. Chen, *ACS Appl. Energy Mater.*, 2019, 2, 4370
102. X. Wang, H. Huang, F. Zhou, P. Das, P. Wen, S. Zheng, P. Lu, Y. Yu, Z.-S. Wu, *Nano Energy*, 2021, 82, 105688
103. K. Zhu, Z. Li, Z. Sun, P. Liu, T. Jin, X. Chen, H. Li, W. Lu, L. Jiao, *Small*, 2022, 18, e2107662
104. S. Liu, T. Lei, Q. Song, J. Zhu, C. Zhu, *ACS Appl. Mater. Interfaces*, 2022, 14, 11425
105. D. Reber, R.-S. Kühnel, C. Battaglia, *ACS Mater. Lett.*, 2019, 1, 44
106. M. Qiu, P. Sun, K. Han, Z. Pang, J. Du, J. Li, J. Chen, Z.-L. Wang, W. Mai, *Nat. Commun.*, 2023, 14, 601
107. Y. Lu, F. Zhang, X. Lu, H. Jiang, W. Hu, L. Liu, L. Gai, *Nanomaterials (Basel)*, 2022, 12, 1920
108. Q. Nian, J. Wang, S. Liu, T. Sun, S. Zheng, Y. Zhang, Z. Tao, J. Chen, *Angew. Chem. Int. Ed.*, 2019, 58, 16994
109. K. Zhu, Z. Sun, Z. Li, P. Liu, X. Chen, L. Jiao, *Energy Storage Mater.*, 2022, 53, 523

110. R.-N. Havemeyer, *J. Pharm. Sci.*, 1966, 55, 851
111. Y. Sun, Y. Zhang, Z. Xu, W. Gou, X. Han, M. Liu, C.-M. Li, *ChemSusChem*, 2022, 15, e202201362
112. H. Bi, X. Wang, H. Liu, Y. He, W. Wang, W. Deng, X. Ma, Y. Wang, W. Rao, Y. Chai, H. Ma, R. Li, J. Chen, Y. Wang, M. Xue, *Adv. Mater.*, 2020, 32, e2000074
113. R. Chua, Y. Cai, P.-Q. Lim, S. Kumar, R. Satish, W. Manalastas, Jr., H. Ren, V. Verma, S. Meng, S.-A. Morris, P. Kidkhunthod, J. Bai, M. Srinivasan, *ACS Appl. Mater. Interfaces*, 2020, 12, 22862
114. J.-Z. Rong, T.-X. Cai, Y.-Z. Bai, X. Zhao, T. Wu, Y.-K. Wu, W. Zhao, W.-J. Dong, S.-M. Xu, J. Chen, F.-Q. Huang, *Cell Rep. Phys. Sci.*, 2022, 3, 100805
115. Q. Wang, C. Zhao, Z. Yao, J. Wang, F. Wu, S.-G. Kumar, S. Ganapathy, S. Eustace, X. Bai, B. Li, *Adv. Mater.*, 2023, 35, 2210677
116. C. Yang, J. Xia, C. Cui, T.-P. Pollard, J. Vatamanu, A. Faraone, J.-A. Dura, M. Tyagi, A. Kattan, E. Thimsen, J. Xu, W. Song, E. Hu, X. Ji, S. Hou, X. Zhang, M.-S. Ding, S. Hwang, D. Su, Y. Ren, X.-Q. Yang, H. Wang, O. Borodin, C. Wang, *Nat. Sustain.*, 2023, 6, 325

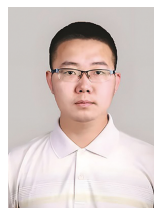


©2023 The Authors. *Energy Lab* is published by Lab Academic Press. This is an open access article under the terms of the Creative Commons Attribution License, which permits use, distribution and reproduction in any medium, provided the original work is properly cited.

Biographies



Tianze Shi obtained his BS degree from Northwest University in 2019, and received his MS degree from the Chongqing Institute of Green and Intelligent Technology, University of Chinese Academy of Science in 2022. He is currently a research assistant at the College of Engineering and Applied Sciences, Nanjing University, and a research assistant in Shenzhen Research Institute of Nanjing University. His research interest focuses on electrolyte design for sodium-ion batteries and related mechanism study.



Ruilin Hou obtained his BS degree from China University of Mining and Technology in 2017, and received his PhD from the Lanzhou Institute of Chemical Physics, University of Chinese Academy of Science in 2022. He is currently a postdoctoral researcher at the College of Engineering and Applied Sciences, Nanjing University, and a research associate in Shenzhen Research Institute of Nanjing University. His research interest focuses on electrolyte design for advanced secondary batteries and related mechanism study.



Shaohua Guo received his PhD from the University of Tsukuba in 2015, after which he worked as a postdoctoral researcher at the National Institute of Advanced Industrial Science and Technology (AIST). He is currently a Professor at the College of Engineering and Applied Sciences, Nanjing University, and a researcher in Shenzhen Research Institute of Nanjing University. His research interest involves energy materials and chemistries for advanced secondary batteries.